JOURNAL OF CHEMICAL & ENGINEERING DATA

ARTICLE

pubs.acs.org/jced

Synthesis, Characterization, and Application in the CO Oxidation over a Copper Nanocatalyst Confined in SBA-15

Vanessa S. Garcia-Cuello,[†] Liliana Giraldo,[†] and Juan Carlos Moreno-Piraján*[,‡]

[†]Facultad de Ciencias, Departamento de Química, Universidad Nacional de Colombia, Bogotá, Colombia

[‡]Facultad de Ciencias, Departamento de Química, Grupo de Investigación de Sólidos Porosos y Calorimetría, Universidad de los Andes, Bogotá, Colombia

ABSTRACT: Copper nanoparticles within the pore channels of selectively grafted mesoporous silica SBA-15 were synthesized. Silanols on the external surface of as-SBA-15 were first capped by $-Si(CH_3)_3$ groups. After the removal of the template of capped SBA-15 by calcination, silanols on the internal surface of SBA-15 were modified by 3-aminopropyltrimethoxysilane (APTMS), and then formaldehyde was grafted to the amino groups of APTMS and with $Cu(NH_3)_4(NO_3)$. The support and catalyst were characterized by X-ray diffraction (XRD), Barett−Joyner−Halenda (BJH) pore-size distribution, Brunauer−Emmett−Teller (BET) surface area, Fourier transform infrared spectroscopy (FT-IR), transmission electron microscopy (TEM), scanning electron microscopy (SEM), and adsorption calorimetry. The initial conversion follows the trend in size: 52 % at pore size 6.0 for this catalyst at 343 K.

INTRODUCTION

Recently, the discovery of mesoporous silicas, such as M41s[1] and SBA-15,[2] has stimulated intensive studies of "host−guest" chemistry inside the channels of mesoporous silicas,[3−6] which have potential applications in catalysis, selective adsorbents, medicine,[7] sensors,[8,9] and nanomaterial fabrications. Thanks to their uniform mesostructures, high surface areas, and tunable pore sizes,[2] these ordered mesoporous silicas have been used as promising templates to control the shape and size of metal nanoparticles.[10−16] Many published works give the relation between nanoparticles confined in various molecular sieves and their properties.[17−19] Moreover, the surface of these ordered mesoporous silicas are also modified for many potential applications. For modifying the mesoporous materials through covalent linkage between functional groups and silica frameworks, two major methods, grafting (post synthesis) and co-condensation (direct incorporation), have been traditionally explored.[20] Grafting is one of the modification methods for presynthesized mesoporous silica, in which the organic functional groups can be introduced by direct reaction of organosilanes to the silica surface. It is up to the application of the thus formed materials, other functionalities can be fixed to the previously introduced functional groups including amino, thiol, and alkyl groups through covalent bonding and/or molecular recognition.[20−23] The distribution and concentration of functional groups are influenced by reactivity of the organosilane and their accessibility to surface silanols, which are limited by diffusion and steric factors. Chao et al.[6,11] prepared SBA-15 functionalized with $(CH_3O)_3Si(CH_2)_3N(CH_3)_3Cl$ (TPTAC) and further synthesized metal nanoparticles by anion exchange between grafted SBA-15 and metal precursors inside the channels as well as upon reduction of precursors. The amount of metal loading as well as the morphology of metal in the host SBA-15 can be rationally controlled through repeating ion exchange/reduction cycles in the TPTAC-SBA-15 silica host. They used the same method to prepare Au nanoparticles and found that the size and morphology of Au nanoparticles in mesoporous SBA-15 are controllable by the preparation methods.

However, the above-mentioned grafting methods basically allow the introduction of functionalization at both intrapore and extrapore media, which led the nanoparticles to form at both surfaces. Therefore, large metal particle aggregates would form on the external surface of the host materials. To overcome this disadvantage, Shi et al.[4] synthesized Pt nanoclusters within the pore channels of selectively modified mesoporous silica SBA-15 by a new in situ reduction process. The silanols on the external surface of SBA-15 were capped with $-Si(CH_3)_3$ groups, thus effectively avoiding the formation of large particles outside the channels. On the other hand, the inner surface of the channel was functionalized with highly reducing Si−H bonds. Pt nanoclusters were formed inside the channels of SBA-15 from H_2PtCl_6 by in situ reduction with Si−H bonds. Recently, Sun et al.[3] have developed a novel in situ auto reduction route to synthesize monodispersed silver nanoparticles inside the channels of SBA-15. Nanoparticles confined in SBA-15 silica possess high catalytic activity and stability because they are stabilizer-free and confined. Jiang et al.[24] found that the Pt nanoparticles confined in SBA-15 exhibit a high electrocatalytic activity toward the oxidation of carbon monoxide (CO) and methanol, and the linearly adsorbed CO species is the only intermediate derived from dissociative adsorption of methanol, which is more readily oxidized to form CO_2 in the aid of the active oxide in SBA-15.

In this paper, stabilizer-free and confined copper nanoparticles inside the channels of selectively grafted mesoporous silica SBA-15

Special Issue: John M. Prausnitz Festschrift

Received: October 25, 2010
Accepted: February 25, 2011
Published: March 15, 2011

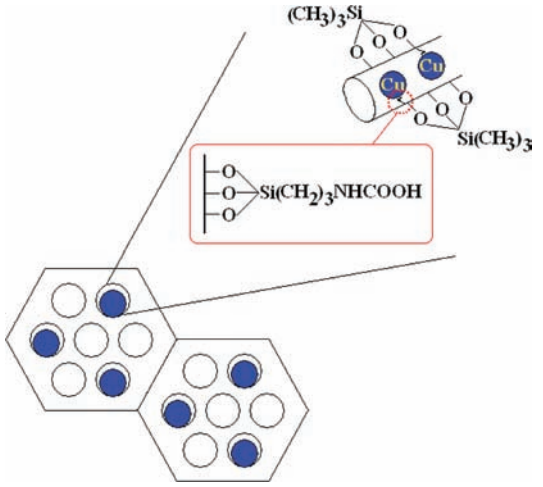

Figure 1. Schematic representation of the synthesis of Cu-SBA-15.

by an in situ reduction process were synthesized according to reported procedures in the literature[25] (see Figure 1). We will show that its catalytic activity in CO oxidation is high compared with the results from catalysts made with other metals.

EXPERIMENTAL SECTION

Synthesis of Cu-SBA-15. As illustrated by Figure 1, mesoporous silica SBA-15 was synthesized following the published procedure[2,25] using the triblock copolymer Pluronic P123 as a template in acid conditions. Typically, a 12.80 g Pluronic P123 template was dissolved with stirring in a solution of 500 mL of 2 M HCl at 313 K, and 27.20 g of tetraethyl orthosilicate (TEOS) was then added. The resulting mixture was stirred at 313 K for 48 h and then aged at 373 K for 72 h under static conditions. The recovered solid was extensively washed with deionized water and drying at 353 K for 24 h and yielded as-SBA-15. To get calcined SBA-15 (cal-SBA-15), the surfactant template of as-SBA-15 was removed by calcination in air at 823 K for 12 h. Cu-SBA-15 was prepared according to the literature procedure.[3,25] The 4.0 g of as-SBA-15 was dispersed in 400 mL of dry toluene under flowing N_2, and then 20 mL of trimethylchlorosilane (TMCS) was added dropwise under stirring. The mixture was filtered with toluene and ethanol after stirring continuously at 353 K for 12 h. After that, the surfactant template was removed by calcination in air at 823 K for 12 h. Thus, SBA-15 with the external surface capped with $-Si(CH_3)_3$ (named cal-TMCS-SBA-15) was collected.

After degassing at 353 K for 24 h, 6.0 g of cal-TMCS-SBA-15 was suspended in 450 mL of dry toluene, and then 18.0 mL of 3-aminopropyltrimethoxysilane (APTMS) was added under stirring. The mixture obtained was stirred for another 24 h at room temperature and refluxed at 353 K for 12 h. The solid was obtained after washing with toluene and then with ethanol intensively to eliminate the physically adsorbed APTMS and toluene. The selectively modified sample after being vacuum-dried at 353 K for 12 h was labeled APTMS-TMCS-SBA-15. To introduce a reducer of formaldehyde into the channels, 2.0 g of APTMS-TMCS-SBA-15 was soaked in a 210 mL mixture of formaldehyde, ethanol, and water (formaldehyde/ethanol/water, 10:40:160, v/v/v), and the suspension was stirred at 313 K for 60 min. The product was filtered, rinsed with deionized water, dried at 323 K for 24 h, and denoted as HCHO-APTMS-TMCS-SBA-15. For Cu incorporation, 6.0 g of HCHO-APTMS-TMCSSBA-15 was added into a mixture of ethanol and 0.02 M $Cu(NH_3)_4(NO_3)$ (aq) (1:6, v/v), respectively, and then the mixture was stirred at 313 K for 60 min. The product was filtered and rinsed thoroughly with deionized water and dried under vacuum at 323 K overnight, and the thus-formed confined copper nanoparticles were labeled as Cu-SBA-15.

Characterization of the Catalyst. The synthesized solid samples were analyzed by different techniques. Scanning electron micrographs were obtained by using a scanning electron microscope JEOL JSM 6510LV. The powder samples were mounted on standard specimen stubs with the help of double adhesive tape and silver paste. The samples were coated with a thin layer of gold in Polaran coating unit E-5000 to prevent the charging of the sample. The electron beam parameters were kept constant during the analysis of the entire sample. The micrograph of the samples with 10 kV EHT and 25 pA beam current were recorded by a 35 mm camera attached on the high resolution recording unit. Transmission electron microscopy (TEM) was carried out with a JEOL JEM 3200FSC, using an acceleration voltage of 300 kV, to analyze the inner pore structures of the SBA-15 materials, the dispersion, and the mean size of active sites on the support surface. Before the analysis, the samples were crushed and ground to a fine power in a gate mortar. Then, the samples were prepared directly and dispersed in ethanol by ultrasound for several min and then dropped on copper grids. The crystalline phases of the SBA-15 materials were identified by resolution X-ray diffractometry (XRD). The spectra were scanned over the range 2θ = 1.0 to 20° at a rate of 1 deg/min. Fourier transform infrared spectra (FT-IR) of the samples were collected in over range of (400 to 4000) cm^{-1}. By functional groups of the infrared absorption spectra, the interspecies bonding could be determined. The adsorption−desorption nitrogen isotherms were measured at the temperature of liquid nitrogen using an Autosorb 3B (Quantachrome, Boyton Beach, MI). The surface area was determined by applying the Brunauer−Emmett−Teller (BET) equation, and the pore size diameter was estimated from the peak position of the Horvath−Kawazoe pore size distribution for cylinder pore geometry (Saito-Foley). Before adsorption, samples were outgassed by heating at 373 K in a vacuum lower than $3 \cdot 10^{-2}$ mm Hg for 12 h.

For the calculation of V_p the proposed method is based on the nonlocal density functional theory (NLDFT) of adsorption and capillary condensation in cylindrical pores. The NLDFT method allows one to calculate the mesopore size distribution and to evaluate the pore wall thickness and the amount of intrawall porosity. The structural parameters obtained by the NLDFT method are in agreement with geometrical considerations. The NLDFT method for the isotherms with a H1 hysteresis loop the two kernels are used for calculations from the experimental (a) desorption branches and (b) adsorption branches.[26] For SBA-15 materials, which exhibit H1 hysteresis loops, both branches of the experimental isotherm are, in principle, applicable for PSD calculations. Because the desorption branch of the experimental isotherm in cylindrical pores is more likely to correspond to thermodynamic equilibrium, it is preferable to employ the desorption branch, provided that it is not affected by networking effects. The hydrothermal stability was tested with catalyst granulated sample grains of (0.4 to 1.0) mm. Then 1 g of catalyst granulated sample was placed in a quartz vertical tube (diameter 11 mm) connected with a vessel containing boiling water under atmospheric pressure. In routine experiments each sample was kept in water vapor at a set temperature for 2 h from (375 to 975) K.

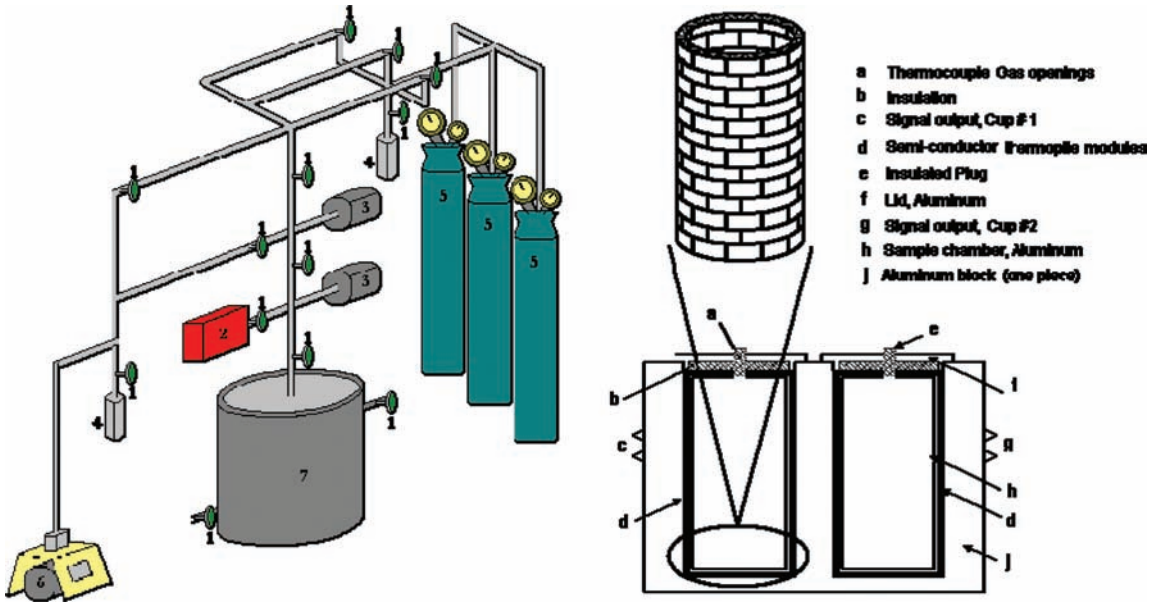

Figure 2. Schematic of an adsorption microcalorimeter: 1, precision valves; 2, calibration volume; 3, pressure transducer of full pressure; 4, cold trap; 5, injection gases; 6, high-vacuum pump; and 7, adsorption microcalorimeter.

After cooling, hydrothermally treated samples were characterized with XRD (AXS D8 Advance from Bruker) nitrogen adsorption−desorption (Autosorb 3B, Quantachrome Boynton Beach, Miami, FL) and temperature programmed desorption (TPD) of ammonia. The surface area for these assays was determined from adsorption isotherms by the BET method, whereas pore volume and their distribution were determined from desorption isotherms by the BJH method. The micropore volume was calculated from the *t*-plot.

Measurement of Differential Heats of CO Adsorption. The differential heats of CO adsorption were measured using a Tian-Calvet heat flow microcalorimeter built in our laboratory.[27−30] Before CO adsorption, the catalysts were reduced at 763 K by H_2 (ordinary pressure, flow rate 30 mL·min^{-1}) for 1 h. After cooling to room temperature, the catalyst sample was transferred to the calorimeter, the system was evacuated to 10 $^{-5}$ Pa, and then $6.6 \cdot 10^4$ Pa H_2 was admitted into the system. The cell was heated to 753 K over a period of 2 h to reduce the catalyst. The gas in the cell was evacuated and replaced with fresh hydrogen two times during the reduction. Following reduction, the catalyst was outgassed at 753 K for 2 h. After cooling the cell to room temperature, the calorimeter thermal block was subsequently raised around the cell, and the system was allowed to equilibrate overnight. A schematic diagram of the microcalorimetric system is shown in Figure 2. The microcalorimeter is capable of operation at temperatures from (77 to 573) K. This microcalorimeter is connected, by means of a specially designed set of calorimeter cells, to a volumetric system equipped with a vacuum system (dynamic vacuum of 10^{-5} Pa), a gas handling system with probe molecule reservoir, and a calibrated dosing volume employing Pfeiffer transducer manometers ($\pm$ $1 \cdot 10^{-5}$ Pa). The leak rate of the volumetric system is 10^{-3} Pa/min in a system volume of approximately 70 cm^3 (i.e., 10^{-4} μmol·min^{-1}).

The microcalorimetric cells are constructed of AISI type 316 stainless steel and measure about 30 cm long and about 5 mm wide. Two identical receptacles in the same material are connected to ends of the cell stems with modified Cajon VCR fittings. The length (10 cm), diameter (5 mm), and distance apart (12 cm) of these receptacles were chosen to match the depth, diameter, and spacing of the transducer wells in the microcalorimeters (Figure 1). The cell calorimeter containing the sample as well as two diffusers were placed along each of the cell stems to minimize convective air currents within the transducer well. A stainless steel holder near the top of the stems, equipped with Viton O-rings, provides a seal between the cell stems and transducer wells, and serves to isolate the cell in the calorimeter. The upper portion of the cells are fitted with a MDC bellows-sealed linear motion feed through fixed to the top of the cells using standard, copper-gasketed, 0.5 in. outside diameter vacuum flanges (MDC). A system of precision valves allows the dosing of the respective amounts of gases. In a typical experiment, a measured mass of sample (typically (0.5 to 2.0) g) is loaded into the glass cell, followed by treatment with the following gases (e.g., calcinations in oxygen) and reduction to the metallic state in hydrogen at elevated temperatures (e.g., 723 K). After the completion of the treatment cycle, the sample is purged with helium (ca. 4 h) at an elevated temperature to remove the adsorbed gases, cooled to room temperature in flowing helium, and subsequently evacuated to ca. $1 \cdot 10^{-4}$ Pa of helium. The sample is then transferred into the stainless steel cell, which is subsequently immersed in the isothermal block. The cells are evacuated to ca. 10^{-4} Pa and allowed to reach thermal equilibrium with the calorimeter (ca. (5 to 6) h), at which point a stable differential heat response (baseline) is achieved. The microcalorimetric measurements are initiated when doses of the adsorbent (doses ca. (10 to 30) μmol) are sequentially admitted to the sample until it becomes saturated. The resulting heat response for each dose is recorded as a function of time and subsequently integrated to determine the amount of heat generated (mJ). The amount of gas adsorbed (μmol·g^{-1}) is determined volumetrically from dose and equilibrium pressures and the system volumes and temperatures. The differential heats (kJ·mol^{-1}), defined as the negative of the enthalpy change of adsorption per mole of gas, are then calculated for each dose by dividing the heat generated by the amount of gas adsorbed.

Catalysis Application. Prior to the catalysis tests, the catalysts are activated by calcinations under air at 560 °C. Then the catalysts were heated to 600 °C under H_2/N_2 flow and held for 1 h and cooled to room temperature under N_2 flow. Oxidation of carbon monoxide was carried out in a quartz-tubular reactor (10 mm i.d.) under atmospheric pressure. Catalysts with a fixed amount of nanoparticles of copper were used for the reaction. Two gases: 32.7 mL·min^{-1} of air and 0.33 mL·min^{-1} of carbon monoxide (99.3 %, CP grade, Linde Division, Union Carbide) were purified by 4 Å molecular sieves and then mixed and flowed into the reactor for the reaction. The water vapor content in the reactant stream is no more than 4 mg·L^{-1}. A HP Agilent 6890 GC gas chromatograph was used for the analysis of the composition in the reactor out-stream. A Carboxy-2000 column was employed for the separation of carbon dioxide, carbon monoxide, nitrogen, and oxygen.

RESULTS AND DISCUSSION

N_2 Adsorption Isotherm. Figure 3 shows an N_2 adsorption−desorption isotherm at 77 K for the Cu-SBA-15 material. Characteristic International Union of Pure and Applied Chemistry (IUPAC) type IV-isotherms with H1 hysteresis loops are depicted for all of these substrates. The range of relative pressures ($p/p°$) at which hysteresis can pack inside the cylindrical channels while not fully occupying the total available space leaves some room for N_2 adsorption. As expected, the presence of metal molecules leads to corresponding decreases in pore diameter, surface area, and pore volume of metal-containing SBA-15 samples (see Table 1).

Data obtained (not published here) for the adsorption−desorption isotherms of nitrogen at 77 K (not shown here) indicate that the hydrothermal stability of nonmodified SBA-15 is rather stable until 575 K. However, the hydrothermal treatments at 675 K for nanostructure of Cu-SBA-15 result in an almost 20 % lower value of the BET surface area.[31] A further increase of temperature up to 775 K causes the surface area to decrease by 50 % and significant changes in micropore volume. Moreover, average pore diameters calculated by the BJH method show an increase. The decrease of pore and micropore volumes with simultaneous increase of average pore diameter after hydrothermal treatment was observed after 2 h of exposure of Cu-SBA-15 in rather extreme hydrothermal conditions. Similar experiments were performed by our research group at room temperature for prolonged exposure of Cu-SBA-15 to water vapor. Significant changes both in the surface area and structure were observed.

IR Results. The framework IR spectrum of calcined Cu-SBA-15 is shown in Figure 4. An adsorption band at ca. 960 cm^{-1} is observed, and a very similar band is also observed in titanium siloxane polymers, mixed oxides, or TiO_2-grafted on silica, which is attributed to a modification of SiO_2 units indirectly relating to the presence of heterometals. Therefore, the IR band at 960 cm^{-1} could be assigned to a Si−O−T (T = Cu) vibration in the Cu-containing SBA-15 framework structure. The IR spectrum of the sample also shows no presence of CuO due to no Cu−O stretch vibration band at 536 cm^{-1}. The results of the XRD and IR testify completely that the Cu was incorporated into the framework sites of the SBA-15.

XRD Results. The XRD patterns of mesoporous copper-containg SBA-15 are shown in Figure 5. The d_{100} spacing, pore

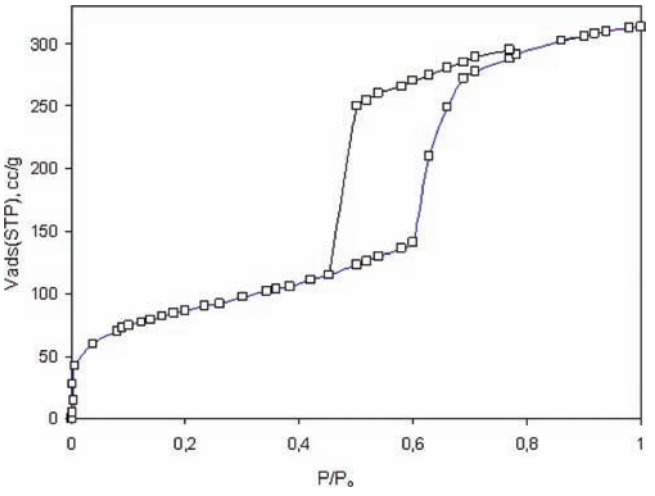

Figure 3. Adsorption isotherms of catalyst: Cu-SBA-15.

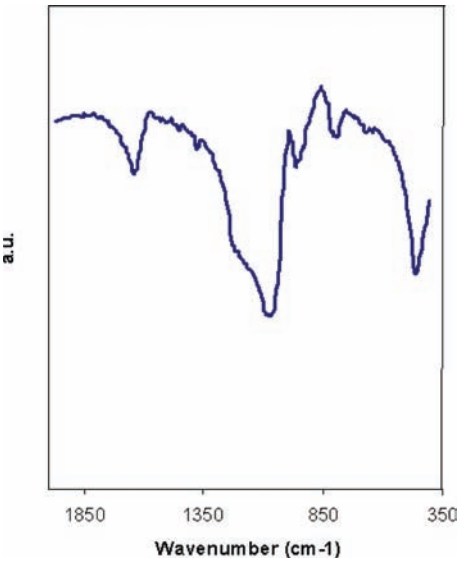

Figure 4. FT-IR spectra of SBA-15 catalyst Cu-SBA-15.

Table 1. Porosity Properties of SBA-15 and Cu-SBA-15 Samples

sample	S_{BET}	S_{microp}	V_P	$V_{P,Microp}$	D_P	h
	$(m^2 \cdot g^{-1})^a$	$(m^2 \cdot g^{-1})^b$	$(cm^2 \cdot g^{-1})^c$	$(cm^2 \cdot g^{-1})^b$	$(nm)^d$	$(nm)^d$
SBA-15	803	176	1.09	0.076	8.5	5.8
Cu-SBA-15	723	125	0.92	0.045	6.0	5.3

[a] Brunauer−Emmett−Teller specific surface area. [b] Micropore surface and volume by the *t*-plot method. [c] Calculated by NLDFT method from the desorption branch. [d] Wall thickness by a_o-D_P.

dx.doi.org/10.1021/je101084w |*J. Chem. Eng. Data* 2011, 56, 1167–1173

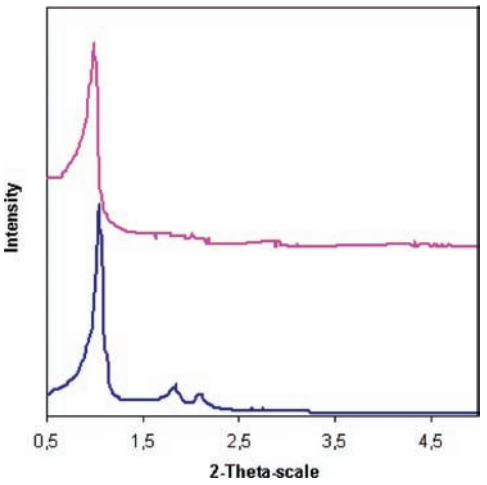

Figure 5. XRD of Cu-SBA-15.

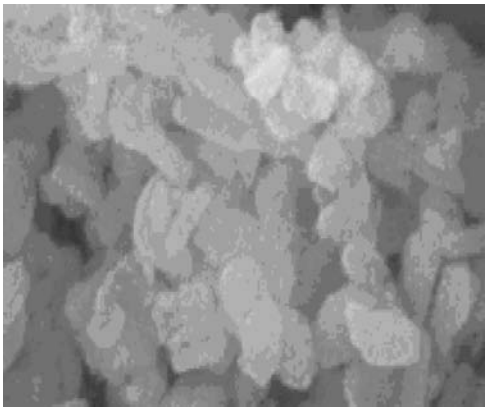

Figure 6. Scanning electron microscope image of Cu-SBA-15.

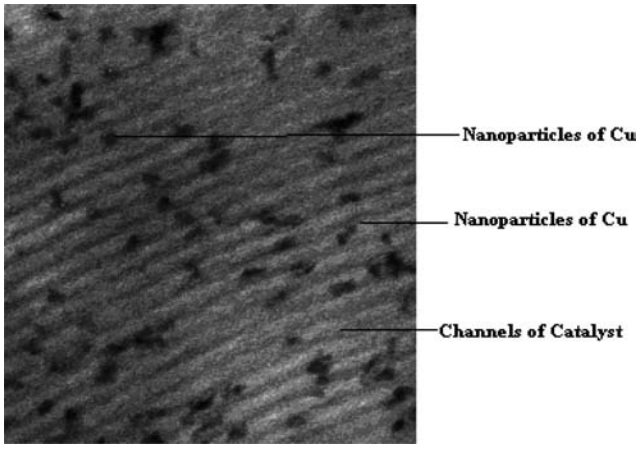

Figure 7. Typical TEM image of Cu-SBA-15 composite (scale 50 nm).

volumes, and unit cell parameters of Cu-SBA-15 and SBA-15 before and after calcination are given in Table 1. The low angle XRD patterns show a prominent peak corresponding to (100) reflections and much weaker, but observable, peaks corresponding to (110) and (200) reflections, which is the typical character of SBA-15 molecular sieves.[32] The unit cell dimensions ($a_o = 2d_{100}(3)^{1/2}$) of

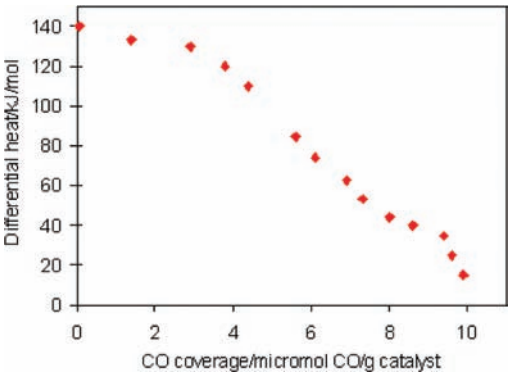

Figure 8. Differential heats of CO adsorption Cu-SBA-15 at 303 K with 3:1 atomic ratios.

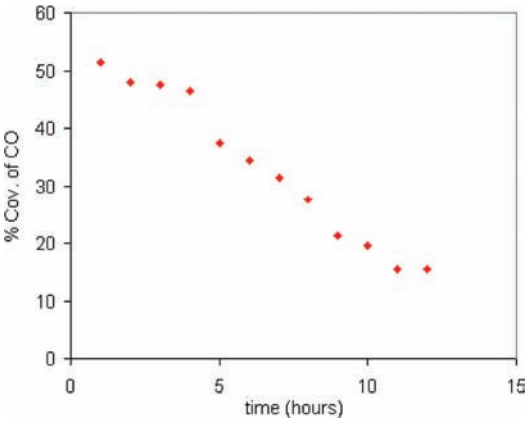

Figure 9. CO conversion percentage of the mesoporous silica containing Cu nanoparticles. The reaction conditions: feed gas 1 % CO weight balanced with air, T = 343 K, and WHSV = $7 \cdot 10^4$ mL·h^{-1}·g^{-1}.

calcined Cu-SBA-15 is 114.3 Å. The higher-angle XRD pattern shows that there is no formation of copper oxide particles (aggregations) in or outside the pores of Cu-SBA-15, which indicates that the product Cu-SBA-15 is in a pure crystal phase, and the Cu may be incorporated into the framework of mesoporous material Cu-SBA-15.

SEM and TEM Results. The SEM images showed that the typical morphology of SBA-15 in the form of cylinders constituted by particles with a wheat grain shape, commonly observed in pure SBA-15 materials, which is conserved after deposition of the nanoparticles of Cu (Figure 6). The morphology of the modified solids is similar to that of pure SBA-15 and is consistent with those obtained in similar studies.[33,34] This technique verified that there were no morphological differences between the obtained silicas.

TEM analysis results of metal/SBA-15 composites are shown in Figure 7. The representative TEM images reveal that (i) the SBA-15 silica materials have a well-ordered mesoporous channel structure, which supports the aforementioned N_2 sorption and low-angle XRD results; (ii) spherical Cu nanoparticles were highly dispersed in the interior of the SBA-15 channels (Figure 7). The average Cu nanoparticle size was determined to be 6.0 nm, with a narrow distribution (i.e., monodispersed) (it is surmised that the pore channels can effectively control the scale of particles formed inside the host).

Differential Heats of Adsorption of CO on Catalyst Cu-SBA-15. The Cu-SBA-15 catalyst, the portion of strong CO adsorption presents a steady stationary at first with an increase of CO coverage and then decreases remarkably when the differential heat of CO adsorption was lower than 125 kJ·mol^{-1} (see Figure 8). The saturation coverage of CO changed dramatically with the adding of Cu nanoparticles to the SBA-15 as support. This result is novel and important in this research. For these Cu-SBA-15 catalysts, 90 % of the adsorbed CO interacted with Cu to produce differential heats of (15 to 140) kJ·mol^{-1}, and no maximum existed, which implies that the main distribution of differential heats of CO adsorption of the Cu-SBA-15 was very broad and homogeneous.

CO Oxidation over the Confined Cu Nanocatalyst in SBA-15 Results. We now discuss the catalytic activities of the Cu-SBA-15 silica systems for CO oxidation. Figure 9 shows that the Cu-SBA-15, with a metal loading of 1 % (by weight), has the capability to catalyze the CO oxidation reaction at 70 °C. The relatively high conversion (∼52 %) in CO oxidation of our treated Cu-SBA-15 catalyst may be due to the small size of the Cu nanoparticles (6.0 nm). The small steady state CO oxidation activity of Cu-SBA-15, as shown in the figure, shows the study of the catalytic activity of this catalyst that lasts 5 h and then drops the conversion percentage after 10 h of catalytic activity to reach the steady state again in a conversion of approximately 20 % of CO. The smaller the size of the Cu nanoparticles, the higher the CO oxidation activity that appears. This is because the many organic groups around the Cu nanoparticles surface prevent the surface of these from being exposed.

The size effect in Cu-SBA-15 catalyzed CO oxidation is an outstanding problem in catalysis.[34−36] It is known that there is an optimum size for CO oxidation of other metals, for example, of Au nanoparticles around 3 nm.[34−36] However, the underlying physical chemistry is not clear yet. A substantial complication arises from the strong effect from the support. The method for deposition of Cu nanoparticles and the kind of oxide used as support affects the catalytic activity. Using standard preparation methods, such as precipitation or impregnation, to deposit Cu nanoparticles on various supports, researchers found that catalytic oxidation of CO with other precious metals, for example, Au nanoparticles supported on silica, is usually not effective. Recently, it was argued that, of the many factors affecting certain metals catalytic activity, the particle size seems to be the dominating one, while catalyst-supported interaction seems to be secondary.[37] The activity of our catalyst is comparable to the best previously reported in the literature, for example, the Au catalyst. We believe that the SBA-15 support does not play an active role in CO oxidation. Thus, the difference in catalytic activity in the mesoporous support system reported in this paper may be ascribed to a size effect. In our experiment, we are limited to analyze only pore sizes corresponding at nanoparticles of copper in the SBA-15. The initial conversion indeed follows the trend in size: 52 % at pore size 6.0 for this catalyst.

■ CONCLUSIONS

On the basis of literature procedures, nanoparticles of copper were synthesized and are contained within the channels of mesoporous silica SBA15 (Cu-SBA-15) and around the walls of the silica. This catalyst was used in the study of CO oxidation with a conversion of 2 %. The important point in the designing of the material has been the stabilization of the Cu nanoparticles by capping them with a quaternary ammonium ion ligand, having at one end a long alkyl chain (to make the Cu nanoparticles compatible with the hexadecyltrimethylammonium template) and at the other end a triethoxysilyl group ready to condense with TEOS during the formation of the material. The reason for this high catalytic activity is most probably the adequate dispersion and stabilization of the Cu nanoparticles within the mesoporous silica host. This is in contrast with reactions in aqueous media where complete catalyst deactivation occurs by collapse of the mesoporous structure. Even though Cu-SBA-15 is not stable in aqueous media, the material may be interesting also for gas phase reactions such as for instance CO oxidation for which supported Cu nanoparticles have been found to be very active. CO adsorption microcalorimetry was employed in the study of Cu-SBA-15 catalysts. The results indicated that the initial differential heat of CO adsorption of the Cu-SBA-15 catalyst was 140 kJ·mol^{-1}.

■ AUTHOR INFORMATION

Corresponding Author

*E-mail: jumoreno@uniandes.edu.co.

Funding Sources

Financial support from the Fondo Especial de Investigaciones "Proyecto Semilla" de la Facultad de Ciencias de la Universidad de los Andes (Colombia) is acknowledged. The authors thank the agreement between the Universidad Nacional de Colombia and Universidad de los Andes (Colombia).

■ REFERENCES

(1) Kresge, C. T.; Leonowicz, M. E.; Roth, W. J.; Vartuli, J. C.; Beck, J. S. Ordered mesoporous molecular sieves synthesized by a liquid-crystal template mechanism. *Nature* **1992**, *359*, 710–712.

(2) Zhao, D.; Feng, J.; Huo, Q.; Melosh, N.; Fredrickson, G. H.; Chmelka, B. F.; Stucky, G. D. Triblock Copolymer Syntheses of Mesoporous Silica with Periodic 50 to 300 Angstrom Pores. *Science* **1998**, *279*, 548–552.

(3) Sun, J.; Ma, D.; Zhang, H.; Liu, X.; Han, X.; Bao, X.; Weinberg, G.; Pfander, N.; Su, D. Toward monodispersed silver nanoparticles with unusual thermal stability. *J. Am. Chem. Soc.* **2006**, *128*, 15756–15764.

(4) Zhang, L.-X.; Shi, J.-L.; Yu, J.; Hua, Z.-L.; Zhao, X.-G.; Ruan, M.-L. A New In-Situ Reduction Route for the Synthesis of Pt Nanoclusters in the Channels of Mesoporous Silica SBA-15. *Adv. Mater.* **2002**, *14*, 1510–1513.

(5) Li, L.; Shi, J.-L.; Zhang, L.-X.; Xiong, L.-M.; Yan, J.-N. A Novel and Simple In Situ Reduction Route for the Synthesis of an Ultra-Thin Metal Nanocoating in the Channels of Mesoporous Silica Materials. *Adv. Mater.* **2004**, *16*, 1079–1082.

(6) Yang, C.-M.; Liu, P.-H.; Ho, Y.-F.; Chiu, C.-Y.; Chao, K.-J. Highly dispersed metal nanoparticles in functionalized SBA-15. *Chem. Mater.* **2003**, *15*, 275–280.

(7) Song, S.-W.; Hidajat, K.; Kawi, S. Functionalized SBA-15 Materials as Carriers for Controlled Drug Delivery: Influence of Surface Properties on Matrix-Drug Interactions. *Langmuir* **2005**, *21*, 9568–9575.

(8) Bai, Y.; Yang, H.; Yang, W.; Li, Y.; Sun, C. Gold nanoparticles-mesoporous silica composite used as an enzyme immobilization matrix for amperometric glucose biosensor construction. *Sens. Actuators, B* **2007**, *124*, 179–186.

(9) Yiu, H. H. P.; Wright, P. A.; Botting, N. P. Enzyme immobilisation using SBA-15 mesoporous molecular sieves with functionalised surfaces. *J. Mol. Catal. B: Enzym.* **2001**, *15*, 81–92.

(10) Song, H.; Rioux, R. M.; Hoefelmeyer, J. D.; Komor, R.; Niesz, K.; Grass, M.; Yang, P.; Somorjai, G. A. Hydrothermal Growth of Mesoporous SBA-15 Silica in the Presence of PVP-Stabilized Pt

Nanoparticles: Synthesis, Characterization, and Catalytic Properties. *J. Am. Chem. Soc.* **2006**, *128*, 3027–3037.

(11) Liu, P.-H.; Chang, Y.-P.; Phan, T.-H.; Chao, K.-J. The morphology and size of nanostructured Au in Au/SBA-15 affected by preparation conditions. *Mater. Sci. Eng., C* **2006**, *26*, 1017–1022.

(12) Chiang, C.-W.; Wang, A.; Mou, C.-Y. CO oxidation catalyzed by gold nanoparticles confined in mesoporous aluminosilicate Al-SBA-15: pretreatment methods. *Catal. Today* **2006**, *117*, 220–227.

(13) Chiang, C.-W.; Wang, A.; Wan, B.-Z.; Mou, C.-Y. High catalytic activity for CO oxidation of gold nanoparticles confined in acidic support Al-SBA-15 at low temperatures. *J. Phys. Chem. B* **2005**, *109*, 18042–18047.

(14) Petkov, N.; Stock, N.; Bein, T. Gold electroless reduction in nanosized channels of thiol-modified SBA-15 material. *J. Phys. Chem. B* **2005**, *109*, 10737–10743.

(15) Asefa, T.; Lennox, R. B. Synthesis of gold nanoparticles via electroless deposition in SBA-15. *Chem. Mater.* **2005**, *17*, 2481–2483.

(16) Zhu, W.; Han, Y.; An, L. Silver nanoparticles synthesized from mesoporous Ag/SBA-15 composites. *Microporous Mesoporous Mater.* **2005**, *80*, 221–226.

(17) Jiang, Y.-X.; Ding, N.; Sun, S.-G. Enhanced IR absorption of CO adsorbed on Pd nanoparticles embedded in the mesoporous molecular sieve SBA-15. *J. Electroanal. Chem.* **2004**, *563*, 15–21.

(18) Lou, Y.; Wang, H.; Zhang, V.; Wang, Y. SBA-15-supported molybdenum oxides as efficient catalysts for selective oxidation of ethane to formaldehyde and acetaldehyde by oxygen. *J. Catal.* **2007**, *247*, 245–255.

(19) Riouxa, R. M.; Songa, H.; Grassa, M.; Habas, S.; Niesz, K.; Hoefelmeyer, J.; Yang, P.; Somorjai, G. Monodisperse platinum nanoparticles of well-defined shape: synthesis, characterization, catalytic properties and future prospects. *Top. Catal.* **2006**, *39*, 168–172.

(20) Vinu, A.; Hossain, K. Z.; Ariga, V. Recent advances in functionalization ofmesoporous silica. *J. Nanosci. Nanotechnol.* **2005**, *5*, 347–371.

(21) Walcarius, A.; Etienne, M.; Lebeau, V. Rate of access to the binding sites in organically modified silicates. 2. Ordered mesoporous silicas grafted with amine or thiol groups. *Chem. Mater.* **2003**, *15*, 2161–2173.

(22) Walcarius, A.; Etienne, M.; Sayen, S.; Lebeau, B. Grafted silicas in electroanalysis: amorphous versus ordered mesoporous materials. *Electroanalysis* **2003**, *15*, 414–421.

(23) Wan, Y.; Zhang, D.; Hao, V.; Zhao, V. Organic groups functionalised mesoporous silicates. *Int. J. Nanotechnol.* **2007**, *4*, 66–99.

(24) Chen, Z.-F.; Jiang, Y.-X.; Wang, Y.; Xu, J.-M.; Jin, L.-Y.; Sun, S.-G. Electrocatalytic oxidation of carbon monoxide and methanol at Pt nanoparticles confined in SBA-15: voltammetric and in situ infrared spectroscopic studies. *J. Solid State Electrochem.* **2005**, *9*, 363–370.

(25) Lin, D.-H.; Jiang, Y.-X.; Wang, Y.; Sun, S.-G. Silver Nanoparticles Confined in SBA-15 Mesoporous Silica and the Application as a Sensor for Detecting Hydrogen Peroxide. *J. Nanomater.* **2008**, *2008*, 1–10.

(26) Smarsly, B.; Thommes, M.; Ravikocih, P. I.; Neimark, A. V. Characterization of Worm-Like Micro- and Mesoporous Silicas by Small-Angle Scattering and High-Resolution Adsorption Porosimetry. *Adsorption* **2005**, *11*, 653–655.

(27) Moreno-Piraján, J. C.; Giraldo, L.; Sapag, K.; Zgrablich, G.; Garcia-Cuello, V. Adsorption micro calorimeter Design and electric calibration. *J. Therm. Anal. Calorim.* **2009**, *97*, 711–715.

(28) Moreno-Piraján, J. C.; Giraldo, L.; Sapag, K.; Zgrablich, G.; Garcia-Cuello, V. Variation of the noise levels in the baseline of an adsorption microcalorimeter. *J. Therm. Anal. Calorim.* **2009**, *97*, 705–709.

(29) Moreno-Piraján, J. C.; Giraldo, L.; Sapag, K.; Zgrablich, G.; Garcia-Cuello, V. A new microcalorimeter of adsorption for the determination of differential enthalpies. *Microporous Mesoporous Mater.* **2009**, *120*, 239–245.

(30) Moreno-Piraján, J. C.; Giraldo, L.; Sapag, K.; Zgrablich, G.; Garcia-Cuello, V. Analysis of the Response of Thermal Sensors in Adsorption Microcalorimetry. *Int. Rev. Chem. Eng.* **2009**, *1*, 243–249.

(31) Galarneau, A.; Nader, M.; Guenneau, F.; Di Renzo, F.; Gedeon, A. Understanding the Stability in Water of Mesoporous SBA-15 and MCM-41. *J. Phys. Chem. C* **2007**, *111*, 8268–8277.

(32) Zhou, C. F.; Wang, Y. M.; Cao, Y.; Zhuang, T. T.; Huang, W.; Chun, Y.; Zhu, J. H. Solvent-free surface functionalized SBA-15 as a versatile trap of nitrosamines. *J. Mater. Chem.* **2006**, *16*, 1520–1528.

(33) Chiang, C.; Wang, A.; Wan, B.; Mou, C. High Catalytic Activity for CO Oxidation of Gold Nanoparticles Confined in Acidic Support Al-SBA-15 at Low Temperatures. *J. Phys. Chem B.* **2005**, *109*, 18042–18047.

(34) Haruta, M.; Daté, M. Advances in the catalysis of Au nanoparticles. *Appl. Catal., A* **2001**, *222*, 427–437.

(35) Haruta, M. When Gold Is Not Noble: Catalysis by Nanoparticles. *Chem. Rec.* **2003**, *3*, 75–87.

(36) Bond, G. C. Gold: a relatively new catalyst. *Catal. Today* **2002**, *72*, 5–9.

(37) Lopez, N.; Janssens, T. V. W.; Clausen, B. S.; Xu, Y.; Mavrikakis, M.; Bligaard, T.; Norskov, J. K. On the origin of the catalytic activity of gold nanoparticles for low-temperature CO oxidation. *J. Catal.* **2004**, *223*, 232–235.